❏ 510

A deep learning-based intelligent decision-making model for tumor and cancer cell identification

Putta Durga, Deepthi Godavarthi
School of Computer Science and Engineering, VIT-AP University, Amaravati, India

Article Info

ABSTRACT

In the current era, the prevalence of common ailments is leading to an increasing number of fatalities. Various infections, viruses, and other pathogens can cause these illnesses. Some illnesses can give rise to tumors that seriously threaten human health. Distinct forms of tumors exist, including benign, premalignant, and malignant, with cancer being present only in malignant forms. Deep learning (DL) algorithms have emerged as one of the most promising methods for detecting cancers within the human body. However, existing models face criticism for their limitations, such as lack of support for large datasets, and reliance on a limited number of attributes from input images. To address these limitations and enable efficient cancer detection throughout the human body, an intelligent decision-making approach model (IDMA) is proposed. The IDMA is combined with the pre-trained VGG19 for improved training. The IDMA analyses convolutional neural network (CNN) layer images for signs of malignancy and rules out false positives. Various performance indicators, like sensitivity, precision, recall, and F1-score, are used to assess the system's performance. The suggested system has been evaluated and proven to outperform similar current systems, achieving an impressive 98.67% accuracy in detecting cancer cells.

Corresponding Author:

Deepthi Godavarthi
School of Computer Science and Engineering, VIT-AP University
Amaravati, Andhra Pradesh, India
Email: deepthi.g@vitap.ac.in

1. INTRODUCTION

Deep learning (DL) plays a crucial role in healthcare systems, especially in the area of disease prediction [1]. As tumors evolve, it becomes harder for current algorithms and models to keep up. In the brain, tumors come in 120 different varieties. There are both rapidly developing and slowly growing cancers. Rapidly expanding tumors, which can progress into cancer, pose the greatest risk to people of all ages. Experts have a hard time using automation to determine where a tumor is in its progression [2]. As time goes on, non-communicable diseases (NCDs) become the leading cause of death worldwide. For a long time now, scientists have been working on AI-based systems that use decision-making strategies to lessen the burden of disease prediction [3]. Disease prediction problems can also be tackled with the use of computer-based clinical decision support systems (CDSSs) [4]. The CDSS can be used to classify the progression of cancer in a wide range of tumor types.

Several different types of automated methods, such as content-based image retrieval (CBIR), have been developed to identify brain cancers. The primary focus of this method is on comparing the outcomes of both low and higher-level visual data extraction from magnetic resonance imaging (MRI) scans [5]. These tiers are utilized in order to lessen the space. Disease prediction using IoT devices at the edge is a common

application of edge computing [6]. Edge-based methods are utilized to locate the true borders of malignancies. Using high-quality photos, cancers can be detected using a model called generative adversarial networks (GAN) [7]. When training on MRI scans of brain tumors, the convolutional neural network (CNN) is crucial for extracting high-quality features from the pictures.

Various approaches, including segmentation, extraction, and detection from MRI images, are utilized to identify tumor regions. Segmentation involves separating the cerebral venous system using a fully automated algorithm [8]. Combining tumor segmentation with CNN yields improved results. Both 3D CNN and U-Net, as segmentation networks, demonstrate superior performance in accurately predicting tumor regions, leading to precise tumor detection [9].

To address the issues raised in [10], we propose intelligent decision-making approach model (IDMA) in this study. The proposed approach was designed with human brain tumor analysis in mind. Now, DL is the most popular choice for a wide variety of sophisticated uses. The primary goals of DL algorithms are speeding up computation and handling massive amounts of data. Input images are analyzed by the pre-trained model for illness patterns. The high-resolution output photos are a result of the sophisticated filters removing noise from the input photographs. In this study, high-resolution images derived from noise filters are used to identify malignant growths. Based on the assessed attributes of tumors, IDMA can identify them as either malignant or benign. To further improve the proposed system, the reinforcement learning method has been implemented. The accuracy and efficiency with which tumors are located are both enhanced by this learning method. Figure 1 is a representation of the IDMA architecture for identifying tumors that are both malignant and benign.
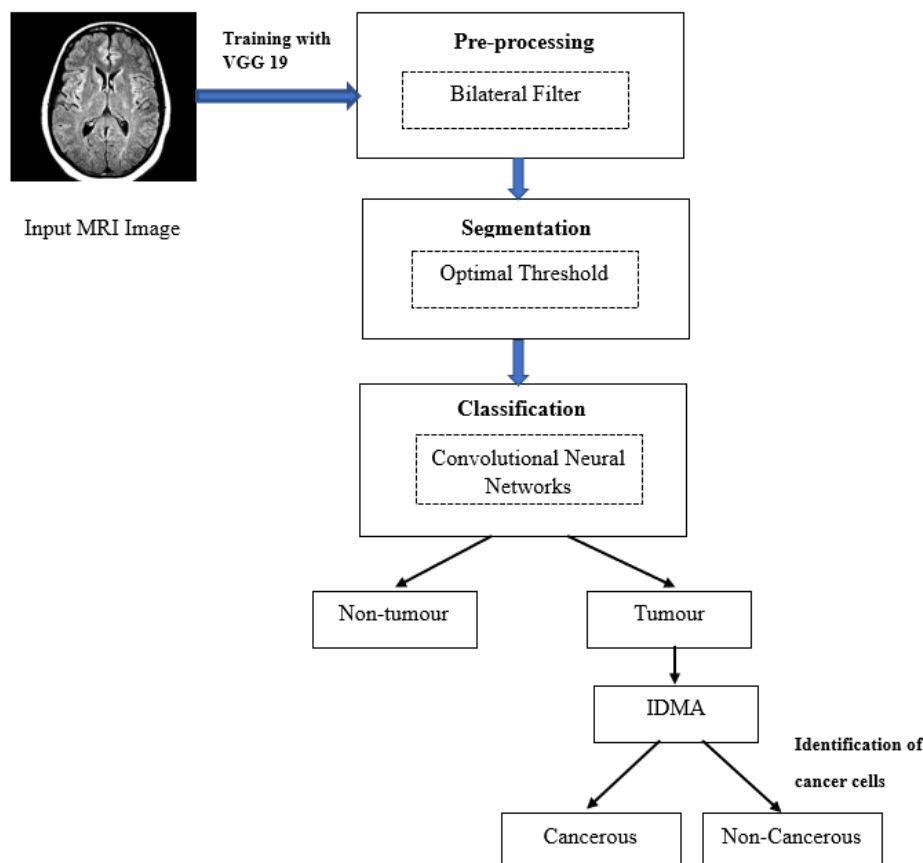

Figure 1. Proposed model framework

In section 1 of the literature review, we examine how disease prognosis is predicted using a variety of existing methodologies that are part of DL models. These algorithms' benefits and weaknesses, as well as how well they function, are discussed. Pre-trained model VGG-19, optimal threshold segmentation, and CNN are all discussed in section 2 of the paper. IDMA and bilateral filter are both explained there. After discussing the implementation outcomes in section 3, a conclusion is presented in section 4.

− Literature survey

Health-cyber-physical system (CPS) was proposed by Zhang *et al*. [11] for designing patient-focused healthcare delivery. The cloud and large amounts of data are integrated into this system. The proposed method involves accumulating several layers. When compared to earlier methods, the CPS's performance was a success. The semantic segmentation strategy was proposed for tongue tumor segmentation by Trajanovski *et al*. [12]. When applied to the HSI data, the proposed method yields reliable outcomes. To identify persistent MB signatures, Hyun *et al*. [13] created a 4-layer CNN. The superior performance of 4-layer CNN can be attributed to its dual-mode channel design. The DL method was proposed by Krijgsman *et al*. [14] for the classification of breast cancers. The author created a method for identifying CD^{8+} cells in breast MRI scans, which are indicative of malignancy. The proposed method also aimed to identify dense areas. The multi-view knowledge-based collaborative (MV-KBC) approach introduced by Xie *et al*. [15] and it can separate cancerous tumor cells from chest computerized tomography (CT) scans. Chest pictures' characteristics were dissected using the 3D lung nodule method. To improve the detection rate, a KBC used ResNet-50 to create three distinct types of image patches. In the end, the results from this model were superior because they were more reliable. The three-step preprocessing technique (PPA) developed by Musallam *et al*. [16] is optimal for MRI scans. Glioma, meningioma, and pituitary tumors were all detected using the deep convolutional neural network (DCNN) employed by the PPA. This model is often referred to as a lightweight model because it contains relatively few layers. The PPA was able to reach 99% accuracy.

The local noise power spectra were used by Divel and Pelc [17] to provide a framework for noise reduction in a given input image (NPS). The fourier transform eliminates noise caused by localized areas by taking the square root of the spatial correlation between them. The spatially correlated noise is used to overlap the patches using the standard deviation. Image compression using a deep wavelet autoencoder (DWA), which combines the default reduction approach with an auto-encoder to break down a wavelet-transformed image, was first introduced by Mallick *et al*. [18]. DNN is combined with the DWA to perform the classification. The DWA-DNN outperforms standard DNN methods in terms of accuracy. Noreen *et al*. [19] introduced a new feature extraction model that diagnoses of brain cancers in the early stages, the performance of the classification technique is enhanced by employing two pre-trained models, namely Inception-v3 and DensNet201.

In order to categorize brain tumors, Gumaei *et al*. [20] created an enhanced approach to extract the characteristics by employing the regularized extreme learning machine (RELM). Edge and location contrast in brain MRI images can be enhanced with the help of the preprocessing approach min-max normalization. The RELM is then used in the categorization process. The proposed strategy outperforms prior methods in terms of classification accuracy.

The combined multi-model fusion and CNN strategy was first introduced by Li *et al*. [21]. This method is a natural progression from 2D-CNN to 3D-CNN, allowing for the use of different model features in 3D space for the extraction of brain lesions. The suggested method incorporates various potential layers, including pooling and the softmax layer, to improve performance. In this case, the loss function is employed to fine-tune the lesion region's improved feature learning. When compared to the 2D-CNN, the accuracy has increased. The hybridized fully convolutional neural network (HFCNN) was proposed by Dong *et al*. [22] and is used for liver tumor segmentation. This method aids in the diagnosis of liver cancer in the patient. The HFCNN is a powerful tool for analyzing liver cancer.

To detect malignancies in MR images, Majib *et al*. [10] presented the VGG-SCN. Images of tumors and healthy tissue are automatically sorted by VGG-SCN. The proposal addresses multiple problems by facilitating faster and more precise work. Khan *et al*. [23] presented new research on a wide range of neurological disorders, including Alzheimer's disease, brain tumors, Parkinson's disease, and more. Several feature extraction methods, pre-trained models, and pre-processing methods are explored. Twenty-two datasets are investigated in this study to identify neurological disorders. Deep learning system (DLS) with data augmentation and transfer learning was proposed by Anaya-Isaza *et al*. [24]. To effectively detect cancers, researchers employ ResNet50, a pre-trained network. Liver tumors were discussed by Zhang *et al*. [25]. Liver tumors might be spotted in a patient's CT scan images. Tumor segmentation is refined using a unique level-set method. The probability distribution of the liver tumor is calculated using fuzzy C-means clustering (FCM) clustering. Segmentation is carried out using this method on two different datasets. Table 1 provides a comparative analysis of various deep learning models, their respective performances, and the datasets utilized in the study.

Table 1. Comparison of existing survey of literature

Study	Model	Dataset	Performance
Trajanovski *et al.* [12]	U-Net	HIS tongue	Dice coefficient and ROC-curve of 0.891 ± 0.053 and 0.924 ± 0.036, Acc-95.8
Xie *et al.* [15]	MV-KBC	LIDC-IDRI	Accuracy-91.60%, AUC-95.70%
Musallam *et al.* [16]	DCNN	Sartaj brain MRI, Navoneel brain tumor	Accuracy-98.22%
Mallick *et al.* [18]	DWA	RIDER neuro MRI	Accuracy-96%
Noreen *et al.* [19]	Inception-v3 and DensNet201	Brain MRI	99.34 and 99.51
Gumaei *et al.* [20]	RELM	Brain MRI	Accuracy-94.23%
Li *et al.* [21]	DenseNet-121	NIH Chest X-ray	AUC-91%
Dong *et al.* [22]	MobileNet-v2	CAMELYON16	Accuracy-91%, AUC-96%
Anaya-Isaza *et al.* [24]	ResNet-50	TCGA-LGG	F1 score-92.34%
Zhang *et al.* [25]	A 2D U-net and a 3D FCN	MICCAI 2017	AUC-97.5%

2. METHOD

In order to detect malignancies in any human tissue, the authors of this research presented an IDDMA. Several procedures are used to identify cancer cells: i) VGG 19, ii) preprocessing with bilateral filter, iii) segmentation, iv) CNNs for classification, and v) cancer cell detection using IDMA. Regarding the extraction of features from the ImageNet dataset, we relied on the VGG19 pre-trained model. The input tumor MRI images are used for segmentation using an optimal threshold, and then the tumor pictures are fed into a CNN for successful classification. The entire process of identifying the tumor and cancer cells process using MRI images of the brain is depicted in Figure 1. Using sophisticated image filters like the bilateral filter, we hope to eliminate the background noise in tumor images (BF). BF's purpose is to smooth pictures and eliminate noise, allowing for clearer visualization of tumors. Then, we used our FBDMA method to locate and detect cancer cells in the provided tumor images. Automatic brain tumor identification will help doctors and nurses quickly diagnose their patients and begin appropriate treatment.

2.1. VGG 19 model

For the provided training images, we utilize a pre-trained model called VGG-19 shown in Figure 2. To provide superior precision in large-scale image processing, this model employs 19 layers of 3×3 convolution filters at a stride of 1. VGG19 is a crucial component of this effort due to its efficacy as a model for accurately extracting features from huge datasets. In this study, we apply VGG19 to improve the precision of brain tumor categorization. The 19 layers of this model are broken down as follows: 16 are convolutional layers used for feature extraction, while 3 are dedicated to picture classification. Each of the five categories of feature extraction layers is called a max-pooling layer. The model's output depicts the object in an input image of 224 by 224 pixels.
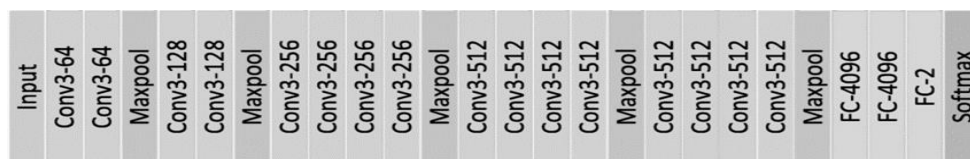

Figure 2. VGG-19 model (from [26])

2.2. Preprocessing

Gaussian measures the dense areas of a bilateral filter, which can be either a constant color or a light color. The emphasis here is similarly on locating the extreme shade variation. The edges of the input image are where this filter shines. Image_I's pixel-level application of a Gaussian filter can be expressed as (1) calculate bilateral filter, $G(p\_x)$:

$$I'(x,y) = (1/Wp) * \sum\sum I(i,j) * wp(i,j) * wd(||I(i,j) - I(x,y)||)\, dxdy \qquad (1)$$

where:
Input image pixel location (x, y) has intensity value (I(x, y)).
The intensity value I'(x, y) of the filtered pixel at coordinates (x, y) in the final image.
The distance between pixel (i, j) and all other pixels is used to calculate the pixel's spatial weight, denoted by wp(I ,j), which is a Gaussian function (x, y).

Pixel (i, j)'s range weight, wd(||I(I ,j) - I(x,y)||), is a Gaussian function of the intensity difference between (i,j) and (x,y). (x, y).

The normalization constant, Wp is the total of the weights for each pair of nearby pixels, both in terms of distance and location.

The pixel brightness in the provided input image was calculated using (2). C is an N-by-N square matrix, where N is the number of grayscale levels. Each ij in the matrix has a specific definition given by (2):

$$C_{ij} = \sum_{a=1}^{W} \sum_{b=1}^{H} 1(I(a, b), i) * 1(I(a + \triangle a, b + \triangle b), j \tag{2}$$

To define the dimensions of the image in terms of its width and height I, 1(I, j), we use the parameters W and H, respectively.

$$I \text{ image } (i, j) = \begin{cases} 1, \text{if } i = j \\ 0, \text{else} \end{cases}$$

If I get a 1, the intensity of the pixels is very high; if I get a 0, the pixel intensity is very low.

2.3. Segmentation

Segmenting an image into its foreground elements and its background elements is what image thresholding does. In this method, pixel values are assigned based on the specified thresholds. Thresholding is typically performed on grayscale images in computer vision.

2.3.1. Optimal threshold

Image threshold is the method used to determine the unique areas in the input MRI image and estimate the threshold values. To minimize segmentation-based pixel misclassification, the best possible threshold is used. The iterative method determines the best threshold for measuring the misclassification loss of a pixel. Background pixel PDF is calculated as follows: assigning a pixel to a class (foreground or background) based on its intensity value and selected threshold results in an error that is quantified by the misclassification loss of a pixel in optimal thresholding. For each given image, the optimal threshold is the value of the threshold that produces the least amount of misclassification. To define the misclassification loss of a pixel in a binary image where 1 and 0 represent the foreground and background classes.
- If a pixel is mislabeled as background while it actually belongs to the foreground class (its true label is 1), the misclassification loss is 1.
- If the pixel's true label is 0 (i.e., it belongs to the background class), and its predicted label is 1 (i.e., it belongs to the foreground class), then the misclassification loss is also 1.
- If the pixel is correctly labeled, the misclassification loss is zero.

2.4. Convolutional neural networks

By training the network using a dataset of tagged pictures of tumor and non-tumor cells, CNN techniques can be used to categorize tumor and non-neoplastic cells. During training, the network is fed a series of images and its weights are adjusted so that the error between the anticipated label and the actual label is as small as possible. The trained network can then be used to label previously unseen images.

The input images are often preprocessed to improve the properties of interest, such as the form, size, and texture of the cells before being used for tumor and non-tumor cell classification. After the photos have been preprocessed, they are given into a CNN, which consists of several convolutional layers to extract features and one or more fully connected layers to do the classification. The last layer produces a probability distribution over tumor and nontumor classes; the class with the highest probability is selected as the anticipated label. To indicate the ReLU's integration in CNN, we write f(k)=max.(0,k).

2.5. Methods used to identify cancer cells

In each determined area, a filtered (noise free) image is captured showing tumors or tumor classifications. Each pixel in the suspected cancerous area has its color intensity calculated and compared to a predetermined threshold; if the pixel's value is lower than the threshold, it is colored black, and if it is higher, it is colored white. Finally, compute the percentage of incorrectly labeled pixels.

Each pixel in an image must be compared with its ground truth labels and its anticipated labels in order to calculate the percentage of erroneously classified pixels. To determine how many correct identifications, incorrect identifications, and false positives and false negatives there were for each pixel, we can utilize a confusion matrix. An illustration of how to determine the fraction of improperly labeled pixels:

i) find the image's pixel count (N) and ii) the number of mislabeled pixels, we can be calculated as follows: $I = FP + FN$, iii) determine the proportion of mislabeled pixels (P) by using the formula: $P = (I / N) \, x \, 100\%$.

Decisions based on the accurate classification of cancer cells using deep learning can have a major impact on patient outcomes. Early detection and diagnosis of cancer can increase the likelihood of a positive outcome from treatment. Moreover, correct categorization of cancer cells might aid in directing therapy decisions and tailoring treatment strategies to patients.

3.   RESULTS AND DISCUSSION

All algorithms were written in the Python programming language and implemented using high-powered library packages such as Pandas, Keras, NumPy, Matplotlib, Seaborn, and scikit-learn, on a computer with high configuration system with 8 GB RAM and 1 TB hard drive with 11th generation system.

3.1. Dataset details

The Br35H dataset can be found in two different files, one for development and one for evaluation. There are a total of 1,000 training MRI pictures, 500 of which are benign and 500 of which are malignant. There are a total of 1,000 MRI scans in the testing folder, 600 of which are of tumors and 400 of which are of healthy tissue; among the 600 tumor scans, some are cancerous and others are not. Apply the confusion matrix to the data, taking into account parameters like sensitivity/recall, accuracy/precision, F1-score, and time in milliseconds. Tables 2 and 3 illustrate the results of a comparison between the performance produced by our proposed model and the performance of existing models for the detection of tumors and cancer cells. In comparison to all of the other models, our suggested model demonstrated superior classification accuracy for malignant and tumorous growths.

Table 2. The performance of different models for detection of tumors cells

Model	Recall	Accuracy	Precision	F1-score	Duration	Error rate
Conv-ML	52.72	54.46	60.15	62.78	17.24	13.32
Hybrid model	81.25	82.42	80.24	82.82	14.64	10.43
IDMA (proposed)	96.77	97.98	98.24	98.66	10.65	7.63

Table 3. The performance of different models for detection of cancer cells

Model	Recall	Accuracy	Precision	F1-score	Duration	Error rate
Conv-ML	63.45	65.78	67.56	65.78	23.34	11.98
Hybrid model	85.12	84.67	86.23	87.12	14.78	8.98
IDMA (proposed)	97.89	98.56	98.78	98.12	7.65	4.12

Figures 3 and 4 display bar graphs indicating the performance of tumor and cancer cell identification. Our proposed model demonstrates superior accuracy compared to other models in the comparison. The steps taken to locate and identify the MRI image of the brain tumor are depicted in Figure 5 and it identifies Figure 5(a) a normal MRI image, Figure 5(b) noise removed image, Figure 5(c) segmented image, and Figure 5(d) tumor affected region. The input image has noise removed using optimal thresholding. The elimination of noise has a noticeable effect on productivity. Partitioning the segmented image follows this process. The input image after noise reduction is used for edge identification to locate the true boundaries of the MRI images. The impacted region of the tumor is shown in red in Figure 5(d).
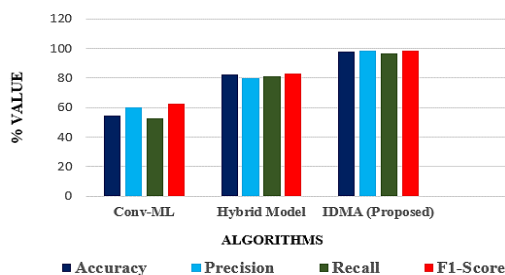

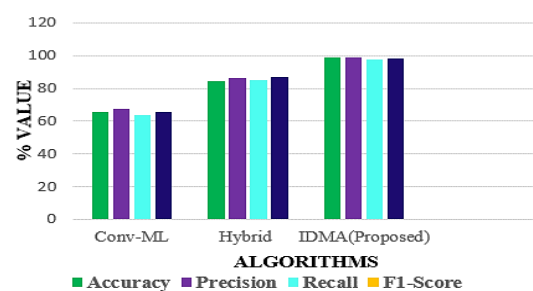Figure 3. Performance of various models for tumor detection

Figure 4. Various models for cancer detection

(a)   (b)   (c)   (d)
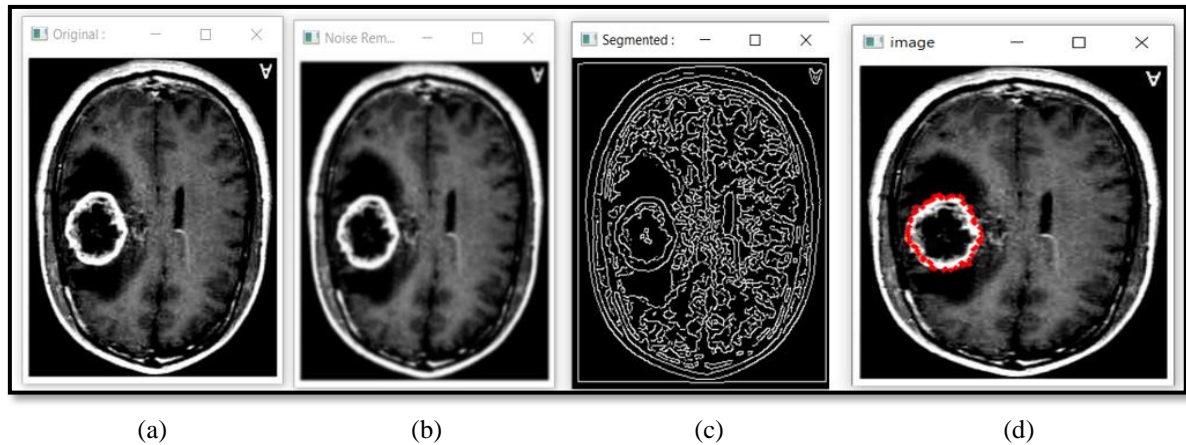
Figure 5. The classification outcome for tumor; (a) a regular image, (b) noise removed, (c) a segmented image, and (d) a tumor

Cancer cells in MRIs of brain tumours can be identified by the steps depicted in Figure 6(a) original MRI, Figure 6(b) noise removal, Figure 6(c) segmented image, and high-intensity areas, which include cancer cells. The blue area in Figure 6(d) represents the cancerous tumor whereas the red area highlights the tumor cell. Finally, the IDMA is used to determine whether or not the tumor is malignant. Training and testing are used to evaluate effectiveness. Among the various approaches analyzed, our model demonstrated the best results in terms of computation time and error rate for the detection of tumors and cancer cells in each iteration, as illustrated in Figures 7-10.

(a)   (b)   (c)   (d)
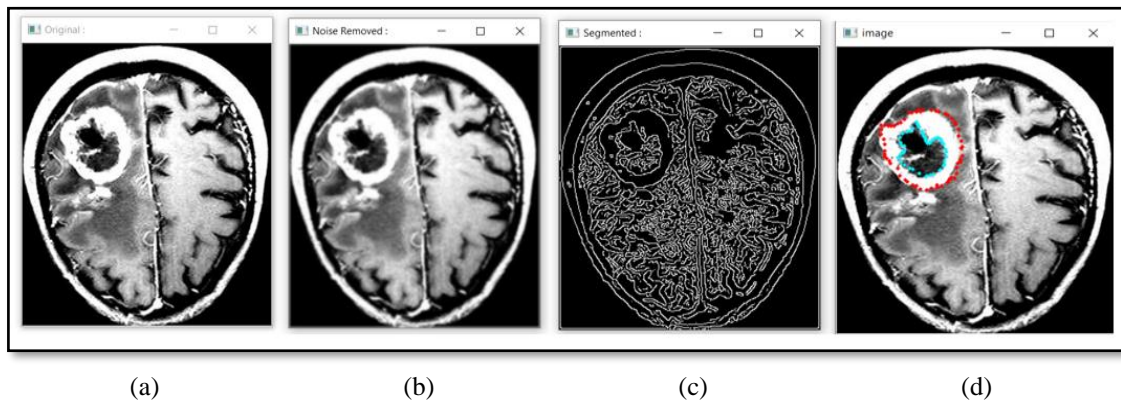
Figure 6. The classification result for cancer cells; (a) image type, (b) noise removed, (c) segmented, and (d) tumor (red) and cancerous cells (blue)
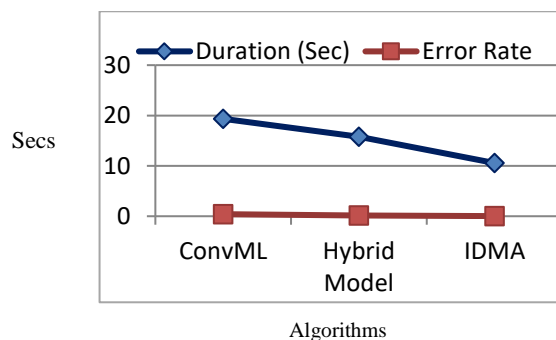

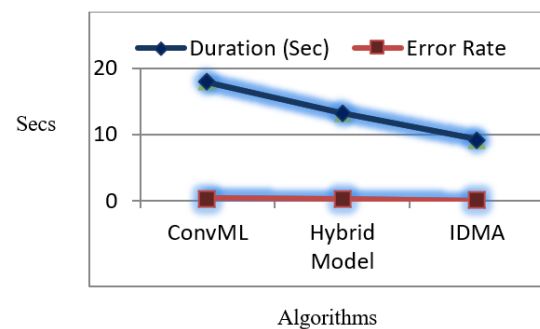Figure 7. Testing time and error rate for tumor

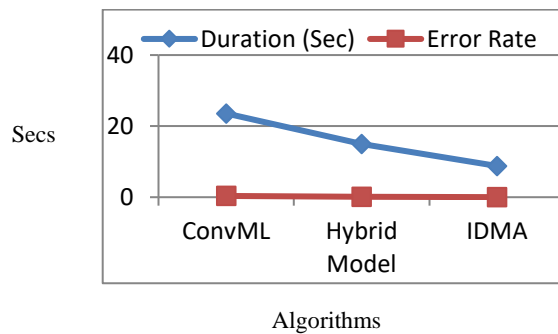Figure 8. Training time and error rate for of tumor images

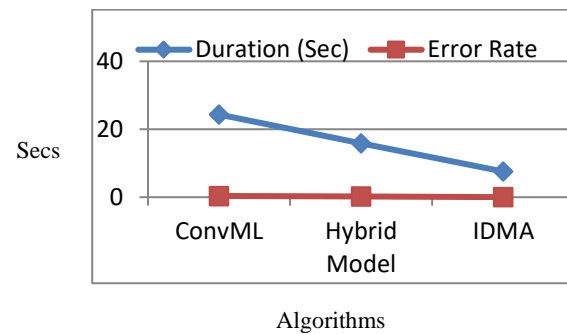Figure 9. Duration and error rate training cancer images

Figure 10. Duration and error rate testing cancer images

4. CONCLUSION

This work employed MRI scans to detect and diagnose brain tumors and cancer cells. IDMA uses the VGG19 pre-trained model for training and feature extraction. Bilateral filters remove photon noise from MRI brain imaging. Optimal threshold segmentation finds normal and abnormal regions in input images. The threshold values define tumors and malignant tumors. CNN extracts feature from MRI brain images to show tumors and malignant tumors. Compared to the Conv-ML and hybrid models, the proposed IDMA accurately identifies tumors and cancer cells with 97.98% and 98.56%. Cancerous areas are blue and tumors red. Every image takes 9.87 seconds to detect tumors and cancer cells.

REFERENCES

[1]   A. Sekhar, S. Biswas, R. Hazra, A. K. Sunaniya, A. Mukherjee, and L. Yang, "Brain Tumor Classification Using Fine-Tuned GoogLeNet Features and Machine Learning Algorithms: IoMT Enabled CAD System," *IEEE Journal of Biomedical and Health Informatics*, vol. 26, no. 3, pp. 983–991, Mar. 2022, doi: 10.1109/JBHI.2021.3100758.

[2]   K. Muhammad, S. Khan, J. Del Ser, and V. H. C. de Albuquerque, "Deep Learning for Multigrade Brain Tumor Classification in Smart Healthcare Systems: A Prospective Survey," *IEEE Transactions on Neural Networks and Learning Systems*, vol. 32, no. 2, pp. 507–522, Feb. 2021, doi: 10.1109/TNNLS.2020.2995800.

[3]   K. Davagdorj, J.-W. Bae, V.-H. Pham, N. Theera-Umpon, and K. H. Ryu, "Explainable Artificial Intelligence Based Framework for Non-Communicable Diseases Prediction," *IEEE Access*, vol. 9, pp. 123672–123688, 2021, doi: 10.1109/ACCESS.2021.3110336.

[4]   H. Yin and N. K. Jha, "A Health Decision Support System for Disease Diagnosis Based on Wearable Medical Sensors and Machine Learning Ensembles," *IEEE Transactions on Multi-Scale Computing Systems*, vol. 3, no. 4, pp. 228–241, Oct. 2017, doi: 10.1109/TMSCS.2017.2710194.

[5]   Z. N. K. Swati *et al.*, "Content-Based Brain Tumor Retrieval for MR Images Using Transfer Learning," *IEEE Access*, vol. 7, pp. 17809–17822, 2019, doi: 10.1109/ACCESS.2019.2892455.

[6]   P. Pace, G. Aloi, R. Gravina, G. Caliciuri, G. Fortino, and A. Liotta, "An Edge-Based Architecture to Support Efficient Applications for Healthcare Industry 4.0," *IEEE Transactions on Industrial Informatics*, vol. 15, no. 1, pp. 481–489, Jan. 2019, doi: 10.1109/TII.2018.2843169.

[7]   M. Mardani *et al.*, "Deep Generative Adversarial Neural Networks for Compressive Sensing MRI," *IEEE Transactions on Medical Imaging*, vol. 38, no. 1, pp. 167–179, Jan. 2019, doi: 10.1109/TMI.2018.2858752.

[8]   Z. Jia and D. Chen, "Brain Tumor Identification and Classification of MRI images using deep learning techniques," *IEEE Access*, p. 1, 2020, doi: 10.1109/ACCESS.2020.3016319.

[9]   M. Ali, S. O. Gilani, A. Waris, K. Zafar, and M. Jamil, "Brain Tumour Image Segmentation Using Deep Networks," *IEEE Access*, vol. 8, pp. 153589–153598, 2020, doi: 10.1109/ACCESS.2020.3018160.

[10]   M. S. Majib, M. M. Rahman, T. M. S. Sazzad, N. I. Khan, and S. K. Dey, "VGG-SCNet: A VGG Net-Based Deep Learning Framework for Brain Tumor Detection on MRI Images," *IEEE Access*, vol. 9, pp. 116942–116952, 2021, doi: 10.1109/ACCESS.2021.3105874.

[11]   Y. Zhang, M. Qiu, C.-W. Tsai, M. M. Hassan, and A. Alamri, "Health-CPS: Healthcare Cyber-Physical System Assisted by Cloud and Big Data," *IEEE Systems Journal*, vol. 11, no. 1, pp. 88–95, Mar. 2017, doi: 10.1109/JSYST.2015.2460747.

[12]   S. Trajanovski, C. Shan, P. J. C. Weijtmans, S. G. B. de Koning, and T. J. M. Ruers, "Tongue Tumor Detection in Hyperspectral Images Using Deep Learning Semantic Segmentation," *IEEE Transactions on Biomedical Engineering*, vol. 68, no. 4, pp. 1330–1340, Apr. 2021, doi: 10.1109/TBME.2020.3026683.

[13]   D. Hyun, L. Abou-Elkacem, R. Bam, L. L. Brickson, C. D. Herickhoff, and J. J. Dahl, "Nondestructive Detection of Targeted Microbubbles Using Dual-Mode Data and Deep Learning for Real-Time Ultrasound Molecular Imaging," *IEEE Transactions on Medical Imaging*, vol. 39, no. 10, pp. 3079–3088, Oct. 2020, doi: 10.1109/TMI.2020.2986762.

[14]   D. Krijgsman *et al.*, "Quantitative Whole Slide Assessment of Tumor-Infiltrating CD8-Positive Lymphocytes in ER-Positive Breast Cancer in Relation to Clinical Outcome," *IEEE Journal of Biomedical and Health Informatics*, vol. 25, no. 2, pp. 381–392, Feb. 2021, doi: 10.1109/JBHI.2020.3003475.

[15]   Y. Xie *et al.*, "Knowledge-based Collaborative Deep Learning for Benign-Malignant Lung Nodule Classification on Chest CT," *IEEE Transactions on Medical Imaging*, vol. 38, no. 4, pp. 991–1004, Apr. 2019, doi: 10.1109/TMI.2018.2876510.

[16]   A. S. Musallam, A. S. Sherif, and M. K. Hussein, "A New Convolutional Neural Network Architecture for Automatic Detection of Brain Tumors in Magnetic Resonance Imaging Images," *IEEE Access*, vol. 10, pp. 2775–2782, 2022, doi:

10.1109/ACCESS.2022.3140289.

[17] S. E. Divel and N. J. Pelc, "Accurate Image Domain Noise Insertion in CT Images," *IEEE Transactions on Medical Imaging*, vol. 39, no. 6, pp. 1906–1916, Jun. 2020, doi: 10.1109/TMI.2019.2961837.

[18] P. K. Mallick, S. H. Ryu, S. K. Satapathy, S. Mishra, G. N. Nguyen, and P. Tiwari, "Brain MRI Image Classification for Cancer Detection Using Deep Wavelet Autoencoder-Based Deep Neural Network," *IEEE Access*, vol. 7, pp. 46278–46287, 2019, doi: 10.1109/ACCESS.2019.2902252.

[19] N. Noreen, S. Palaniappan, A. Qayyum, I. Ahmad, M. Imran, and M. Shoaib, "A Deep Learning Model Based on Concatenation Approach for the Diagnosis of Brain Tumor," *IEEE Access*, vol. 8, pp. 55135–55144, 2020, doi: 10.1109/ACCESS.2020.2978629.

[20] A. Gumaei, M. M. Hassan, M. R. Hassan, A. Alelaiwi, and G. Fortino, "A Hybrid Feature Extraction Method With Regularized Extreme Learning Machine for Brain Tumor Classification," *IEEE Access*, vol. 7, pp. 36266–36273, 2019, doi: 10.1109/ACCESS.2019.2904145.

[21] M. Li, L. Kuang, S. Xu, and Z. Sha, "Brain Tumor Detection Based on Multimodal Information Fusion and Convolutional Neural Network," *IEEE Access*, vol. 7, pp. 180134–180146, 2019, doi: 10.1109/ACCESS.2019.2958370.

[22] X. Dong, Y. Zhou, L. Wang, J. Peng, Y. Lou, and Y. Fan, "Liver Cancer Detection Using Hybridized Fully Convolutional Neural Network Based on Deep Learning Framework," *IEEE Access*, vol. 8, pp. 129889–129898, 2020, doi: 10.1109/ACCESS.2020.3006362.

[23] P. Khan *et al.*, "Machine Learning and Deep Learning Approaches for Brain Disease Diagnosis: Principles and Recent Advances," *IEEE Access*, vol. 9, pp. 37622–37655, 2021, doi: 10.1109/ACCESS.2021.3062484.

[24] A. Anaya-Isaza and L. Mera-Jimenez, "Data Augmentation and Transfer Learning for Brain Tumor Detection in Magnetic Resonance Imaging," *IEEE Access*, vol. 10, pp. 23217–23233, 2022, doi: 10.1109/ACCESS.2022.3154061.

[25] Y. Zhang *et al.*, "Deep Learning Initialized and Gradient Enhanced Level-Set Based Segmentation for Liver Tumor From CT Images," *IEEE Access*, vol. 8, pp. 76056–76068, 2020, doi: 10.1109/ACCESS.2020.2988647.

[26] W. Wang, J. Tian, C. Zhang, Y. Luo, X. Wang, and J. Li, "An improved deep learning approach and its applications on colonic polyp images detection," *BMC Medical Imaging*, vol. 20, no. 1, pp. 1–14, Dec. 2020, doi: 10.1186/s12880-020-00482-3.

BIOGRAPHIES OF AUTHORS

Putta Durga 🆔 📄 SC ⟳ currently pursuing a Ph.D. program at the School of Computer Science and Engineering (SCOPE), VIT–AP University, situated in Amaravati, Andhra Pradesh, India. Her ongoing research focuses on the domains of decision making, machine learning, digital image processing, and NLP. She can be contacted at email: pdurga593@gmail.com.

Deepthi Godavarthi 🆔 📄 SC ⟳ received a Ph.D. degree from Andhra University, Andhra Pradesh, India, in 2022. She is currently working as an Assistant Professor in the School of Computer Science and Engineering at VIT-AP University, Amaravati, AP, India. Her research interests include AI, NLP, computer vision, and block chain technologies. She can be contacted at email: deepthi.g@vitap.ac.in.